J. Fluid Mech. (2001), *vol.* 437, *pp.* 367–384. Printed in the United Kingdom

A numerical comparison between the multiple-scales and finite-element solution for sound propagation in lined flow ducts

By SJOERD W. RIENSTRA[1] AND WALTER EVERSMAN[2]

[1] Department of Mathematics and Computing Science, Eindhoven University of Technology, PO Box 513, 5600 MB Eindhoven, The Netherlands

[2]Department of Mechanical and Aerospace Engineering and Engineering Mechanics, University of Missouri-Rolla, USA

(Received 30 June 1999 and in revised form 16 October 2000)

An explicit, analytical, multiple-scales solution for modal sound transmission through slowly varying ducts with mean flow and acoustic lining is tested against a numerical finite-element solution solving the same potential flow equations. The test geometry taken is representative of a high-bypass turbofan aircraft engine, with typical Mach numbers of 0.5–0.7, circumferential mode numbers m of 10–40, dimensionless wavenumbers of 10–50, and both hard and acoustically treated inlet walls of impedance $Z = 2 - \mathrm{i}$. Of special interest is the presence of the spinner, which incorporates a geometrical complexity which could previously only be handled by fully numerical solutions. The results for predicted power attenuation loss show in general a very good agreement. The results for iso-pressure contour plots compare quite well in the cases where scattering into many higher radial modes can occur easily (high frequency, low angular mode), and again a very good agreement in the other cases.

1. Introduction

The calculational complexities of the multiple-scales solution for modal sound transmission through slowly varying ducts with mean flow and acoustic lining (presented in Rienstra 1998, 1999), are no greater than for the classical modal solution for a straight duct. The multiple-scales solution is an approximation utilizing the axial slope of the duct walls as small parameter. This slope is, for aerodynamical reasons, invariably small in any aero-engine duct.

Therefore, this multiple-scales solution provides an interesting alternative in aero-engine applications, as it allows for both the advantages of the analytical approach (speed of calculation and relative simplicity of programming), and variable geometries including spinner and mean flow variation.

The final approximation error in realistic geometries, however, is difficult to determine, because the number of other parameters involved is rather large (axial, radial, and circumferential wavenumbers, cut-off ratio, wall impedance, Mach number) and some of them are typically large. In particular the frequencies of interest in a modern turbofan engine are high, yielding in general high dimensionless wavenumbers. It is therefore of interest to directly compare the analytical approximation with a fully numerical solution of the same physical model. This is the subject of the present paper.

As a first step towards exploring the possibilities, a series of tests is carried out, comparing the analytical results with results of the finite-element solution, given in Danda Roy & Eversman (1995), of a compressible inviscid isentropic irrotational mean flow, superimposed by linear acoustic perturbations.

2. Physical model

We consider a circular symmetrical duct with a compressible inviscid perfect isentropic irrotational gas flow, consisting of a mean flow and acoustic perturbations. To the mean flow the duct is hard-walled, but for the acoustic field the duct is lined with an impedance wall. In view of the adopted aero-engine geometry, the inner wall (corresponding to the spinner) will be hard-walled, without lining.

We make the following non-dimensionalizations: spatial dimensions on a typical duct radius R_∞, densities on a reference value ρ_∞, velocities on a reference sound speed c_∞, time on R_∞/c_∞, pressure on $\rho_\infty c_\infty^2$, and velocity potential on $R_\infty c_\infty$. Note that the corresponding reference pressure p_∞ satisfies $\rho_\infty c_\infty^2 = \gamma p_\infty$, where $\gamma = 1.4$ is the (constant) ratio of specific heats at constant pressure and volume.

The fluid in the duct is described by

$$\tilde\rho_t + \nabla\cdot(\tilde\rho\tilde{\boldsymbol v}) = 0, \quad \tilde\rho(\tilde{\boldsymbol v}_t + \tilde{\boldsymbol v}\cdot\nabla\tilde{\boldsymbol v}) + \nabla\tilde p = 0, \quad \gamma\tilde p = \tilde\rho^\gamma, \quad \tilde c^2 = \frac{\mathrm{d}\tilde p}{\mathrm{d}\tilde\rho} = \tilde\rho^{\gamma-1} \qquad (1a\text{–}d)$$

(with boundary and initial conditions), where $\tilde{\boldsymbol v}$ is particle velocity, $\tilde\rho$ is density, $\tilde p$ is pressure, $\tilde c$ is sound speed (all dimensionless).

Since we assumed the flow to be irrotational, we may introduce a velocity potential $\tilde\phi$, such that $\tilde{\boldsymbol v} = \nabla\tilde\phi$, and the above momentum equation may be integrated to a variant of Bernoulli's equation

$$\frac{\partial\tilde\phi}{\partial t} + \tfrac{1}{2}|\tilde{\boldsymbol v}|^2 + \frac{\tilde c^2}{\gamma-1} = \text{const.} \qquad (2)$$

This flow is split up into a stationary mean flow part, and an acoustic perturbation. This acoustic part varies harmonically in time with circular frequency ω, and with small amplitude to allow linearization.

In the usual complex notation we write then

$$\tilde{\boldsymbol v} = \boldsymbol V + \boldsymbol v\,\mathrm{e}^{\mathrm{i}\omega t}, \quad \tilde\phi = \Phi + \phi\,\mathrm{e}^{\mathrm{i}\omega t}, \quad \tilde\rho = D + \rho\,\mathrm{e}^{\mathrm{i}\omega t}, \quad \tilde p = P + p\,\mathrm{e}^{\mathrm{i}\omega t}, \quad \tilde c = C + c\,\mathrm{e}^{\mathrm{i}\omega t}.$$

Substitution and linearization yields:

mean flow field

$$\nabla\cdot(D\boldsymbol V) = 0, \quad \tfrac{1}{2}|\boldsymbol V|^2 + \frac{C^2}{\gamma-1} = E, \quad C^2 = \gamma P/D = D^{\gamma-1}; \qquad (3a,b,c)$$

acoustic field

$$\mathrm{i}\omega\rho + \nabla\cdot(D\nabla\phi + \rho\boldsymbol V) = 0, \quad \mathrm{i}\omega\phi + \boldsymbol V\cdot\nabla\phi + \frac{p}{D} = 0, \quad p = C^2\rho, \qquad (4a,b,c)$$

where E is a constant, and the acoustic perturbation of $\tilde c$ is further ignored. The integration constant in equation (4b) may be absorbed by ϕ. For the mean flow the duct wall is solid, so the normal velocity vanishes at the wall. The subsonic mean flow is determined by conditions of uniformity upstream, the constant E, and a constant axial mass flux πF.

For the acoustic part the outer duct wall is a locally reacting impedance wall with

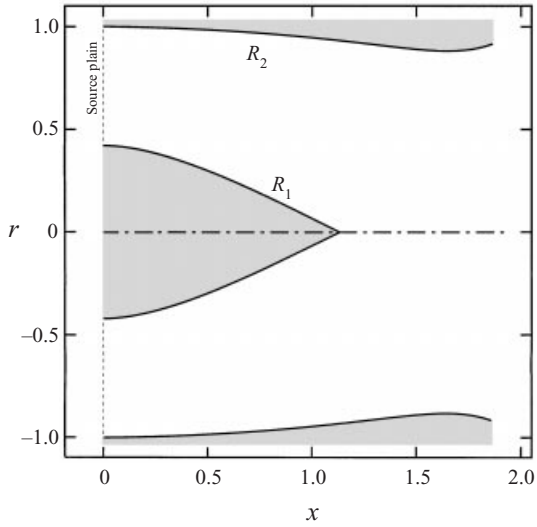

FIGURE 1. Geometry.

complex impedance Z_2. The pertaining boundary condition is for a point near the wall but still (just) inside the mean flow. For arbitrary mean flow along a (smoothly) curved wall, with normal $\boldsymbol{n}$ directed into the wall, this was given by Myers (1980, equation 15), as

$$\mathrm{i}\omega(\boldsymbol{v}\cdot\boldsymbol{n}) = [\mathrm{i}\omega + \boldsymbol{V}\cdot\nabla - \boldsymbol{n}\cdot(\boldsymbol{n}\cdot\nabla\boldsymbol{V})]\left(\frac{p}{Z}\right). \tag{5}$$

3. Geometry

The reference values taken for non-dimensionalization are at the source plane $x = 0$, including the outer radius for length scale.

The outer radius R_2 and inner radius R_1 are described by the following formulae:

$$R_2(x) = 1 - 0.18453x'^2 + 0.10158\,\frac{\mathrm{e}^{-11(1-x')} - \mathrm{e}^{-11}}{1 - \mathrm{e}^{-11}}, \tag{6}$$

$$R_1(x) = \max\,[0, 0.64212 - (0.04777 + 0.98234x'^2)^{1/2}], \tag{7}$$

where $x' = x/L$ and $L = 1.86393$ is the length of the duct; see figure 1.

The mean flow is selected such that at the source plane $x = 0$ the Mach number Ma is equal to -0.5, and the dimensionless density and sound speed equal to 1. The corresponding axial Mach number and dimensionless density variation (based on the quasi-one-dimensional mean flow solution; see below) is depicted in figure 2.

4. Multiple-scales solution

For the existence of the analytical solution it is essential that the mean flow and the acoustic field are approximated on the same footing. An arbitrary, *ad hoc*, mean flow field would not allow the present explicit solution. So the mean flow used for the multiple-scales solution is not exactly the same as the one used for the finite-element solution. They are, however, in terms of approximation of the same level. Therefore, we give here the mean flow and the acoustic field together.

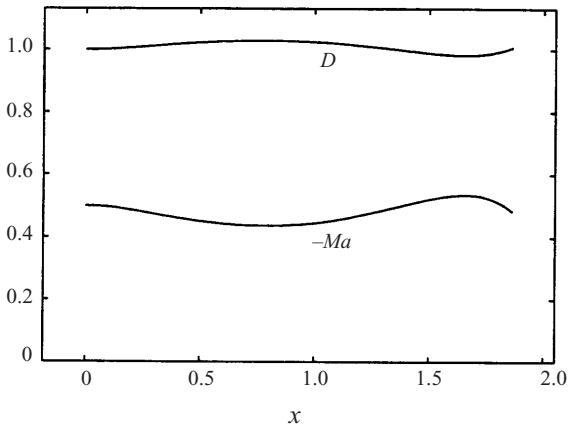

FIGURE 2. Axial Mach number Ma and density D.

The approximation is based on the assumption that geometry and mean flow vary slowly, i.e. on a length scale much larger than a typical duct diameter or wavelength. This is, of course, for aerodynamical reasons the case inside an aero-engine inlet duct. We introduce the ratio between a typical diameter and this length scale as the small parameter ε, and rewrite the duct surface (in radial coordinates (x, r, θ)) as

$$r = R_1(X), \quad r = R_2(X), \quad X = \varepsilon x. \tag{8}$$

By rewriting $R_{1,2}$ as a function of slow variable X, rather than x, we have made our formal assumption of slow variation explicit in a convenient and simple way. Although in the final result ε will play no explicit rôle, a representative value of ε will be necessary for an order of magnitude estimate of the approximation error.

By assuming that the mean flow is nearly uniform with axial variations in X only, we find that small axial mass variations can only be balanced by a small radial flow, so

$$\boldsymbol{V} \simeq U_0(X)\boldsymbol{e}_x + \varepsilon V_1(X, r)\boldsymbol{e}_r$$

and similarly $P \simeq P_0(X)$, $D \simeq D_0(X)$, and $C \simeq C_0(X)$ to leading order are only dependent on X. It follows that

$$U_0(X) = \frac{F}{D_0(X)(R_2^2(X) - R_1^2(X))}$$

with V_1, D_0, P_0 and C_0 given by the well-known one-dimensional gas flow equations (see e.g. Rienstra 1998, 1999).

The acoustic field is assumed to be described by mode-like solutions of the form

$$\phi(x, r, \theta; \varepsilon) = A(X, r; \varepsilon) \exp\left(-\mathrm{i}m\theta - \mathrm{i}\int^x \mu(\varepsilon\xi)\,\mathrm{d}\xi\right), \tag{9}$$

also known as the WKB assumption. After expanding $A = A_0 + \varepsilon A_1 + O(\varepsilon^2)$ and $\mu = \mu_0 + O(\varepsilon^2)$ (any possible μ_1 can be absorbed by A_1), and substitution in equations and boundary conditions, we find for A_0 a Bessel-type equation in r, so we obtain the slowly varying mode

$$A_0 = N(X)J_m(\alpha(X)r) + M(X)Y_m(\alpha(X)r) \tag{10}$$

where J_m and Y_m are the mth-order Bessel function of the first and second kind.

Radial eigenvalue α and M/N are determined by the boundary conditions, yielding

$$\frac{\alpha R_2 J'_m(\alpha R_2) - \zeta_2 J_m(\alpha R_2)}{\alpha R_2 Y'_m(\alpha R_2) - \zeta_2 Y_m(\alpha R_2)} = \frac{\alpha R_1 J'_m(\alpha R_1) + \zeta_1 J_m(\alpha R_1)}{\alpha R_1 Y'_m(\alpha R_1) + \zeta_1 Y_m(\alpha R_1)} = -\frac{M(X)}{N(X)},$$

where

$$\zeta_i = \Omega^2 D_0 R_i / \mathrm{i}\omega Z_i, \quad \alpha^2 + \mu^2 = \Omega^2 / C_0^2, \quad \Omega = \omega - \mu U_0.$$

By solving this eigenvalue equation for μ in sufficiently small steps of X, the integral over μ in equation (9) can be determined by numerical quadrature.

The crux of the solution is the determination of amplitude $N(X)$, as a function of X. This is determined by the next-order equation for A_1. It is, however, not necessary to solve this complicated equation. A solvability condition (Rienstra 1998, 1999) is enough to generate a differential equation in X for N, which can be solved exactly. The general solution for the annular cylinder is given by

$$\left(\frac{\frac{1}{2}\pi Q_0}{N}\right)^2 = \frac{\dfrac{D_0\omega\sigma R_2^2}{2C_0}\left(1 - \dfrac{m^2 - \zeta_2^2}{\alpha^2 R_2^2}\right) + \dfrac{D_0 U_0}{\Omega}\zeta_2}{\left(\alpha R_2 Y'_m(\alpha R_2) - \zeta_2 Y_m(\alpha R_2)\right)^2} - \frac{\dfrac{D_0\omega\sigma R_1^2}{2C_0}\left(1 - \dfrac{m^2 - \zeta_1^2}{\alpha^2 R_1^2}\right) - \dfrac{D_0 U_0}{\Omega}\zeta_1}{\left(\alpha R_1 Y'_m(\alpha R_1) + \zeta_1 Y_m(\alpha R_1)\right)^2}, \quad (11)$$

where Q_0 is an integration constant, and $\sigma^2 = 1 - (C_0^2 - U_0^2)\alpha^2/\omega^2$.

For a hollow cylinder, without an inner wall ($R_1 \equiv 0$, $M \equiv 0$), this general solution reduces to

$$\left(\frac{Q_0}{N}\right)^2 = \left(\frac{D_0\omega\sigma R_2^2}{2C_0}\left(1 - \frac{m^2 - \zeta_2^2}{\alpha^2 R_2^2}\right) + \frac{D_0 U_0}{\Omega}\zeta_2\right) J_m(\alpha R_2)^2. \quad (12)$$

So the present solution is equally valid for hollow and annular cylindrical ducts.

5. Finite-element solution

A numerical model for sound propagation is based on a finite-element discretization of the steady flow field equations (3*a–c*) and the acoustic field equations (4*a–c*). The weak formulation of equation (3*a*) for the steady compressible flow in the duct is in terms of the steady flow velocity potential Φ and steady flow density D,

$$\iiint_V \nabla W \cdot (D\nabla\Phi)\,\mathrm{d}V = \iint_S W(D\nabla\Phi)\cdot\boldsymbol{n}\,\mathrm{d}S. \quad (13)$$

Weighting functions W are from the class of continuous functions on the volume V of the duct bounded by the duct surface S, which includes the duct walls and source and terminal planes. A solution for Φ is sought in the class of continuous functions. The unit normal is directed out of the duct. The duct geometry and the steady flow field are axially symmetric, favouring the introduction of a cylindrical coordinate system with x-axis coincident with the axis of symmetry, r-axis in the source plane at $x = 0$, and the angular coordinate θ locating the r-axis in the $x = 0$ plane (see figure 3 for the computational domain). The steady flow field is represented

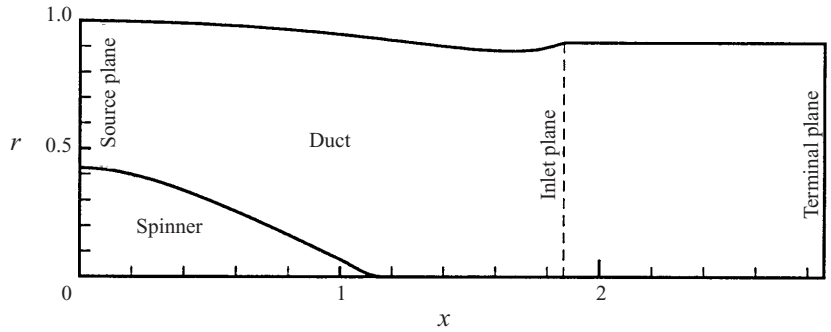

FIGURE 3. Computational domain for the finite-element method.

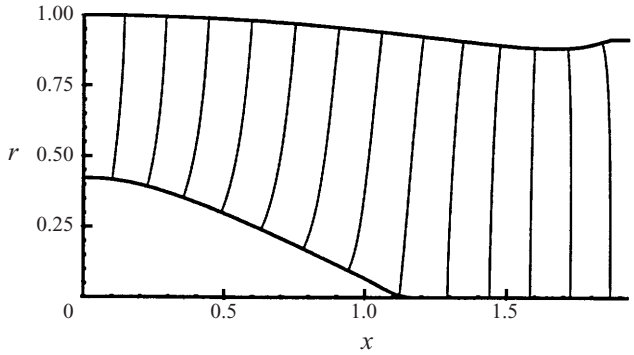

FIGURE 4. Mean flow iso-potential contours.

in an (x, r)-plane, and is two-dimensional. A standard finite-element formulation of equation (13) is based on eight-node isoparametric serendipity elements.

Equations (3*b*) and (3*c*) are subsidiary relations that are used in an iterative solution in which at each stage the finite-element discretization of equation (13) is solved with a density and speed of sound field derived from the previous iteration step. The boundary integral on the right-hand side, which is a natural boundary condition, specifies the mass flow rate on the source plane. A forced boundary condition setting the level of the potential is required on the terminal plane (figure 3). It is assumed that the source plane and terminal plane are located remotely enough from regions of non-uniformity in the duct so that at the source and terminal planes the mean flow velocity is uniform, permitting the natural and forced boundary conditions to be easily implemented. In practical calculations for the type of duct considered this turns out not to be restrictive.

Figure 4 shows mean flow iso-potential contours (of Φ) for the duct described by equations (6) and (7) with a uniform Mach number at the source plane $Ma = -0.5$, directed from right to left (an inlet flow). The duct shape defined by equations (6) and (7) begins at the source plane $x = 0$ and is extended beyond the nominal termination (the 'inlet plane') used in the analytical development in a uniform duct to allow the flow field to become uniform at the terminal plane. No extension is used at the source end and the extension at the exit end is probably longer than necessary. $\boldsymbol{V} = \nabla\Phi$, C, D are required data for the finite-element solution for acoustic propagation.

A finite-element model for acoustic propagation is based on a weak formulation

of equations (4*a–c*). Acoustic perturbations in pressure, density and velocity potential are harmonic in time with frequency ω and harmonic in the angular coordinate θ of the form $p(x,r)\mathrm{e}^{\mathrm{i}\omega t-\mathrm{i}m\theta}$, $\rho(x,r)\mathrm{e}^{\mathrm{i}\omega t-\mathrm{i}m\theta}$, and $\phi(x,r)\mathrm{e}^{\mathrm{i}\omega t-\mathrm{i}m\theta}$. The weak formulation (Danda Roy & Eversman 1995) is

$$\iiint_V \{\nabla W\cdot(D\nabla\phi+\rho\nabla\Phi)-\mathrm{i}\omega W\rho\}\,\mathrm{d}V=\iint_S W(D\nabla\phi+\rho\nabla\Phi)\cdot\boldsymbol{n}\,\mathrm{d}S. \tag{14}$$

The weighting functions are taken as $W(x,r)\mathrm{e}^{\mathrm{i}m\theta}$. Angular harmonics proportional to $\mathrm{e}^{-\mathrm{i}m\theta}$ represent the decomposition of the solution periodic in θ in a Fourier series. The angular mode number m is a parameter of the solution. The surface integral is over all surfaces bounding the domain. The unit normal for the surface integral is out of the domain at the surface in question. The weak formulation continues with the linearized momentum equation (4*b*) and linearized equation of state (4*c*), by rewriting equation (14) in the form

$$\begin{aligned}\iiint_V \frac{D}{C^2}\{&C^2\nabla W\cdot\nabla\phi-(\boldsymbol{V}\cdot\nabla W)(\boldsymbol{V}\cdot\nabla\phi)\\&+\mathrm{i}\omega[W(\boldsymbol{V}\cdot\nabla\phi)-(\boldsymbol{V}\cdot\nabla W)\phi]-\omega^2W\phi\}\,\mathrm{d}V\\&=\iint_S\frac{D}{C^2}\{C^2W\nabla\phi-\boldsymbol{V}W(\boldsymbol{V}\cdot\nabla\phi)-\mathrm{i}\omega\boldsymbol{V}W\phi\}\cdot\boldsymbol{n}\,\mathrm{d}S.\end{aligned} \tag{15}$$

Note that the local steady flow dimensionless velocity $\boldsymbol{V}$ is equivalent to the reference Mach number $\boldsymbol{M}_r$ which in fact is the local steady flow velocity divided by the speed of sound at the source plane.

The surface integral on the right-hand side of equation (15) is the natural boundary condition. On the duct walls this provides the boundary condition for either rigid walls (the integral vanishes) or for a normally reacting lining with an impedance specified by equation (5).

A new formulation of the Myers boundary condition, described in Eversman (2001*b*), which is exact in the finite-element context, has been used to implement equation (5). Details of the finite-element method procedure for discretization of equation (15) can be found in Astley & Eversman (1983), Parrett & Eversman (1986), Eversman *et al.* (1985), Danda Roy & Eversman (1995), and Eversman & Okunbor (1998). The discussion of the implementation of the impedance boundary condition in Eversman & Okunbor (1998) includes approximations not used in the present analysis.

On the source plane and terminal plane the natural boundary condition is used to introduce the noise source and non-reflecting boundary conditions. On these planes the acoustic potential is recast via an eigenmode expansion such that the acoustic potential is given in terms of the complex amplitudes of the right and left propagating acoustic duct modes appropriate for the geometry and flow conditions which prevail there (Eversman 1991). On the source plane, $x=0$ in the present study, right propagating modal amplitudes at the source plane are specified via a forced boundary condition. Left running (reflected) modal amplitudes at the source plane and right running modal amplitudes at the terminal plane are unknown and part of the solution. Left running modal amplitudes at the terminal plane are forced to vanish, imposing a non-reflecting boundary condition. Details of the modal boundary condition are available in Eversman & Baumeister (1986).

Finite-element discretization for acoustic propagation is carried out on the same grid with the same element type as used in the steady flow model. Required data

generated in the steady flow representation are transferred directly to the acoustic analysis. Mesh density is governed by the demands of the acoustic problem and is substantially more refined than would be required in the steady flow analysis.

The finite-element solution proceeds with the computation of the acoustic potential field. Post-processing by the use of equation (4*b*) generates the acoustic pressure field. The solution also includes reflected modal amplitudes and transmitted modal amplitudes. Acoustic power reflection and transmission characteristics are computed directly from the input modal amplitudes and computed reflected and transmitted modal amplitudes. Reciprocity characteristics of the scattering matrices and acoustic power balances are also monitored as a check of computational accuracy in the case of acoustically lined and unlined duct walls (Eversman 2001*a*).

Post-processed acoustic pressures are represented on iso-pressure amplitude contour plots superimposed on the duct geometry. Comparison of finite-element and multiple-scales results is based on visual comparison of these contours, but perhaps more importantly on the basis of computed power transmission coefficients.

6. Differences between multiple-scales and finite-element formulations

There are differences between the multiple-scales solution and the finite-element model, although the field equations (3*a–c*) and (4*a–c*), and Myers' impedance boundary condition (5) are exactly the same in both cases.

The finite-element (FEM) formulation admits the propagation of many modes and therefore scattering is an integral part of the solution. This is manifested by reflection of the incident mode and other modes which are not incident as well as the transmission of modes which are not incident. This will be clearly seen in examples which are presented.

The multiple-scales method utilizes the fact that in a slowly varying duct any scattering of one mode into other modes should be small. The principal manifestation of the propagating sound is still mode-like, albeit not in the strict sense of self-similar straight duct modes, but as locally mode-like solutions with slowly varying amplitude and phase. Each such 'mode' will by (WKB) assumption not scatter into other modes in the slowly varying part of the duct. The scattering into other modes at abrupt changes of the geometry (like the inlet) may be included by traditional methods like mode-matching, but this is not done in the present implementation. Scattering is therefore not a feature of the multiple-scales solution. In particular, since in each test run only one mode is considered, no interference with other modes will occur.

The FEM solution requires the source to be represented in terms of input modal amplitudes for eigenmodes for a duct with hard walls. The source is always located in a section of the duct which has rigid walls. Acoustic treatment is not present exactly at the source plane, although it can be initiated an arbitrarily small distance from the source. This is done because properties of the rigid-wall duct modes (namely, orthogonality) are important in the implementation of the source boundary conditions. Eigenmodes in a duct with an impedance boundary are not orthogonal in the usual sense. The net effect is that there is always a transition from a rigid wall to an impedance wall at both ends of the duct in the FEM model. For mathematical consistency this transition is required to be continuous, but can be made arbitrarily abrupt, approximating a discontinuous change from rigid to impedance wall.

In the multiple-scales analysis the general solution is built up from a summation over slowly varying modes. The natural way to test its validity is therefore to study a single, soft-wall, mode. In order to generate an equivalent input in the FEM model

it is necessary to represent the soft-wall eigenmode as an expansion of hard-wall eigenmodes. A single-mode multiple-scales analysis is therefore described, at the source, by a modal sum of hard-wall modes in the FEM solution. Since the sound field, presented to the lined duct, 'fits' directly into one soft-wall mode, only little reflection at the source plane is to be expected.

Finally, it is noted that the FEM model requires conditions at the source plane which include reflected modal amplitudes, and at the termination plane which force a reflection-free termination (or specified or computed reflection characteristics). These conditions are physically real characteristics of duct propagation, but never appear in the multiple-scales solution where left and right running waves are already given explicitly.

It is not possible to make FEM and multiple-scales models exactly equivalent, nor should it be, since the multiple-scales solution is an approximation based on well-documented assumptions. It is a goal of the numerical comparisons to be given here to investigate how successfully the multiple-scales solution represents the more accurate FEM model, under conditions representative of a modern turbofan engine.

7. Results

The 24 cases considered are grouped as six series of iso-pressure contour plots (figures 5–10), where in each case the first radial mode is input with and without flow, and with a hard and a soft wall. The left-hand column of figures 5–10 displays the numerical FEM solution, the right-hand column the analytical MS (multiple-scales) solution. 'Soft wall' denotes an outer wall impedance $Z_2 = 2 - \mathrm{i}$. The spinner is always hard-walled. 'Flow' denotes a mean flow with Mach number -0.5 at the source plane. 'First radial mode' denotes the mode with smallest real part of radial eigenvalue α at the source plane.

The typical grid size used in the FEM calculations is at or near 5 elements per shortest convected wavelength, which is found in the forward direction (against the flow). The typical number of calculated points for the MS results is 200×200 or 300×300, and the numerical integration of $\int \mu \, \mathrm{d}\xi$ (trapezium method) is based on the same x-grid. This is much higher than necessary, but it made the contour plots smoother, and calculation time was no restriction.

Although in reality the impedance would always vary with frequency, we have restricted ourselves to two wall impedances (∞ = hard wall, and $2 - \mathrm{i}$). We have experimented with other values but they did not seem to produce essentially different results. Similarly, we have considered only a mean flow of Mach number -0.5, and 0 (no flow), as any other Mach number in between would not produce essentially different results. Note that this is not the case for a mean flow of higher Mach number, especially near 1, as such a flow will have in reality supersonic pockets in the throat. However, such cases fall outside the scope of the present MS solution, as transonic flows are poorly represented by the MS mean flow approximation.

As variations in frequency ω and circumferential mode number m yield the biggest effect, these parameters are varied as indicated, and the values are chosen such that they are representative of aircraft engines, probably the most important area of application of flow duct acoustics.

The selected cases do not show turning point behaviour (hard-wall cut-on/cut-off transition). This was excluded because the field with a turning point has not yet been implemented in the MS solution, since the matching of the turning point region (typically described by Airy functions) and the regular acoustic regions (typically

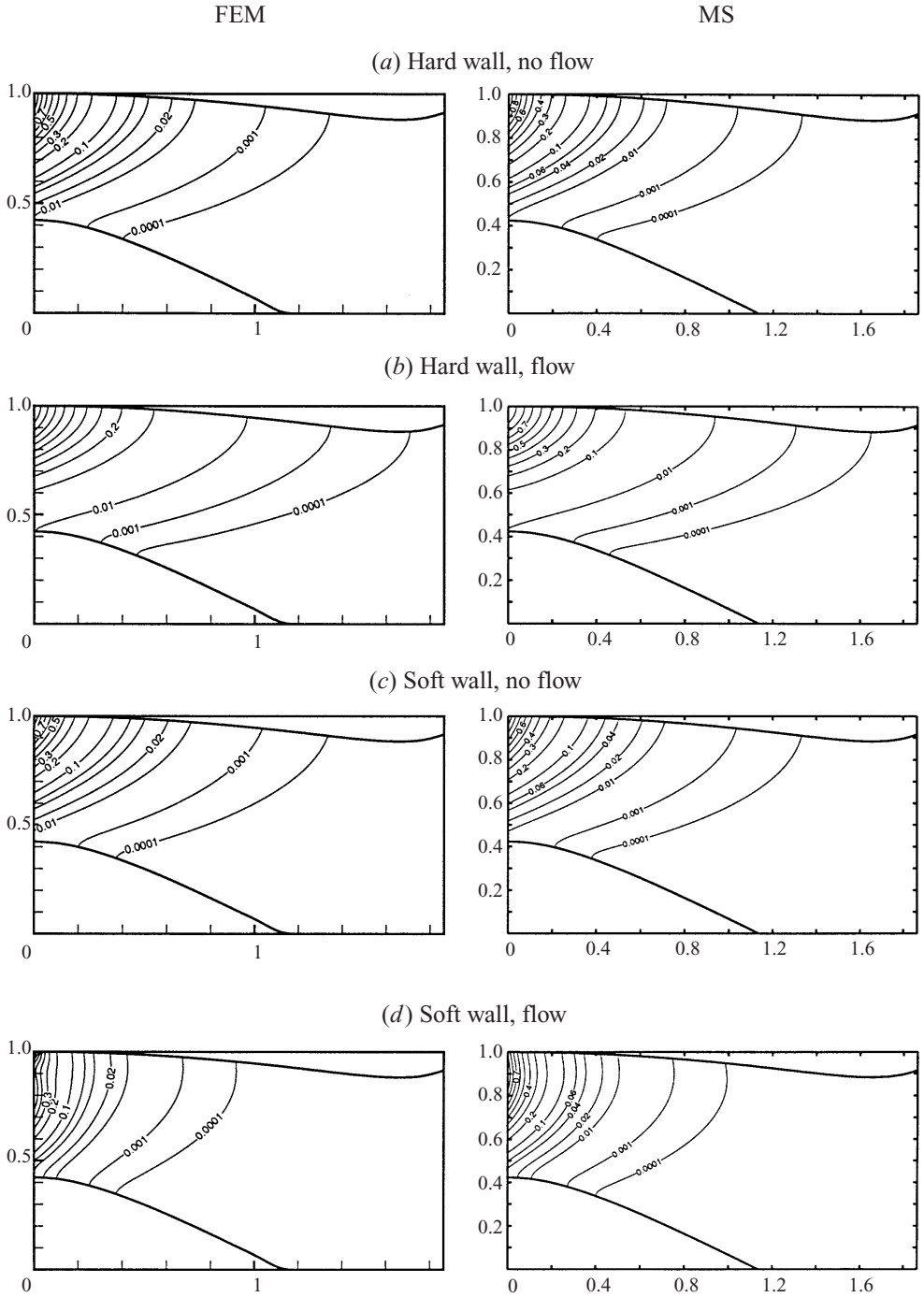

FIGURE 5. Iso-pressure contour plots: comparison between finite-element (FEM) and multiple-scales (MS) solutions where the first radial mode is input, with and without flow and with a hard and soft wall. $m = 10$, $\omega = 10$.

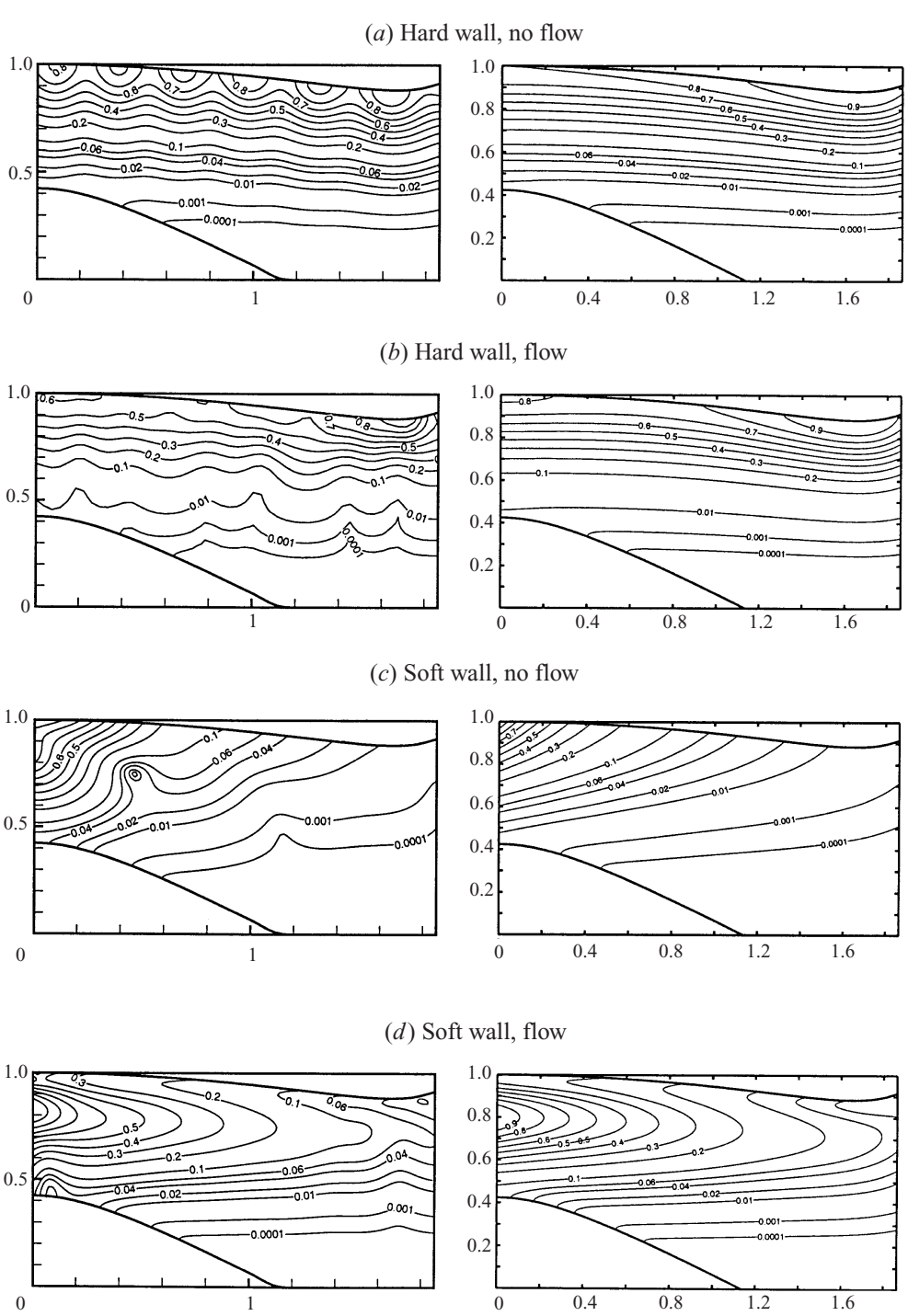

FIGURE 6. As figure 5 but for $m = 10$ and $\omega = 16$.

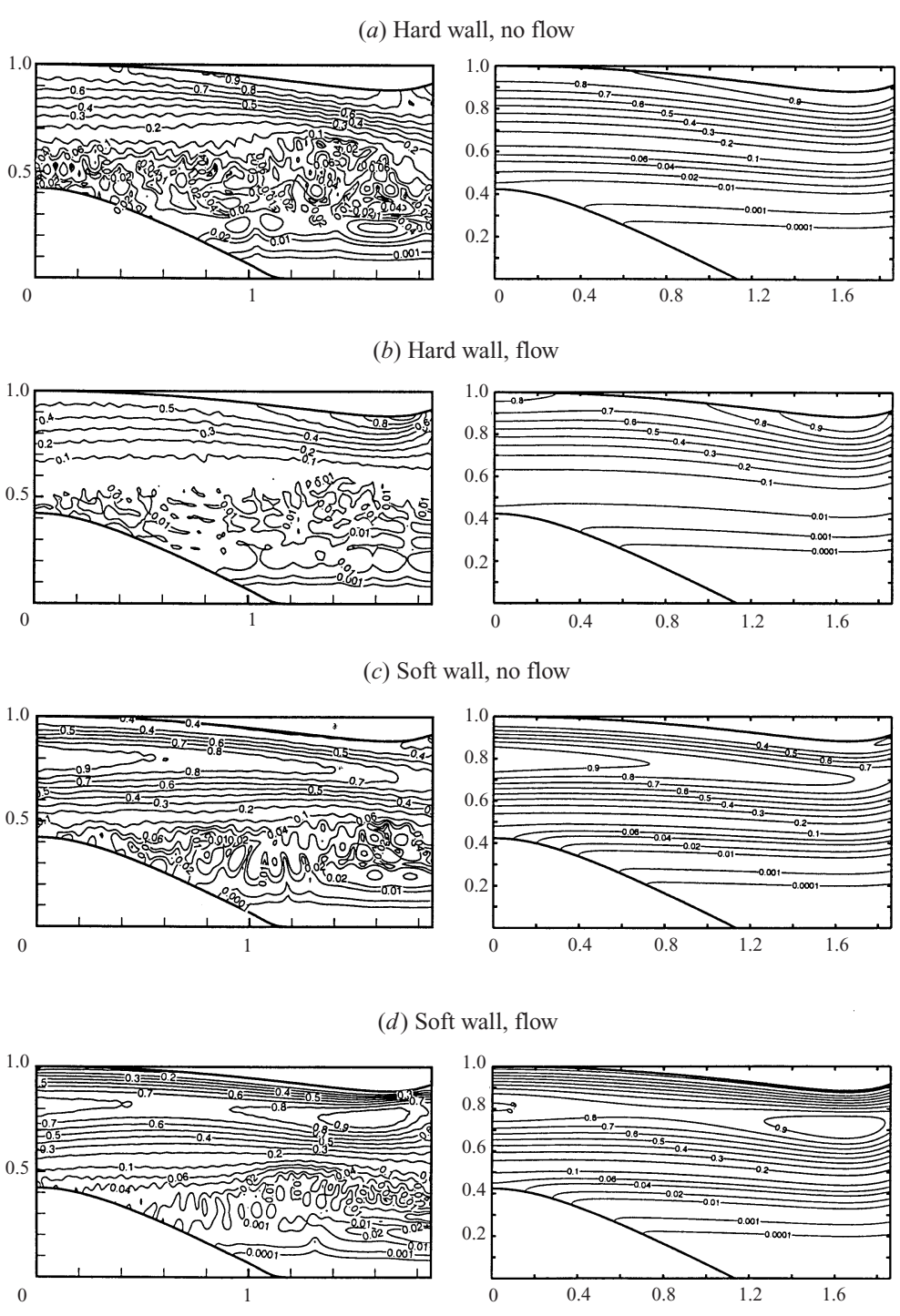

FIGURE 7. As figure 5 but for $m = 10$ and $\omega = 50$.

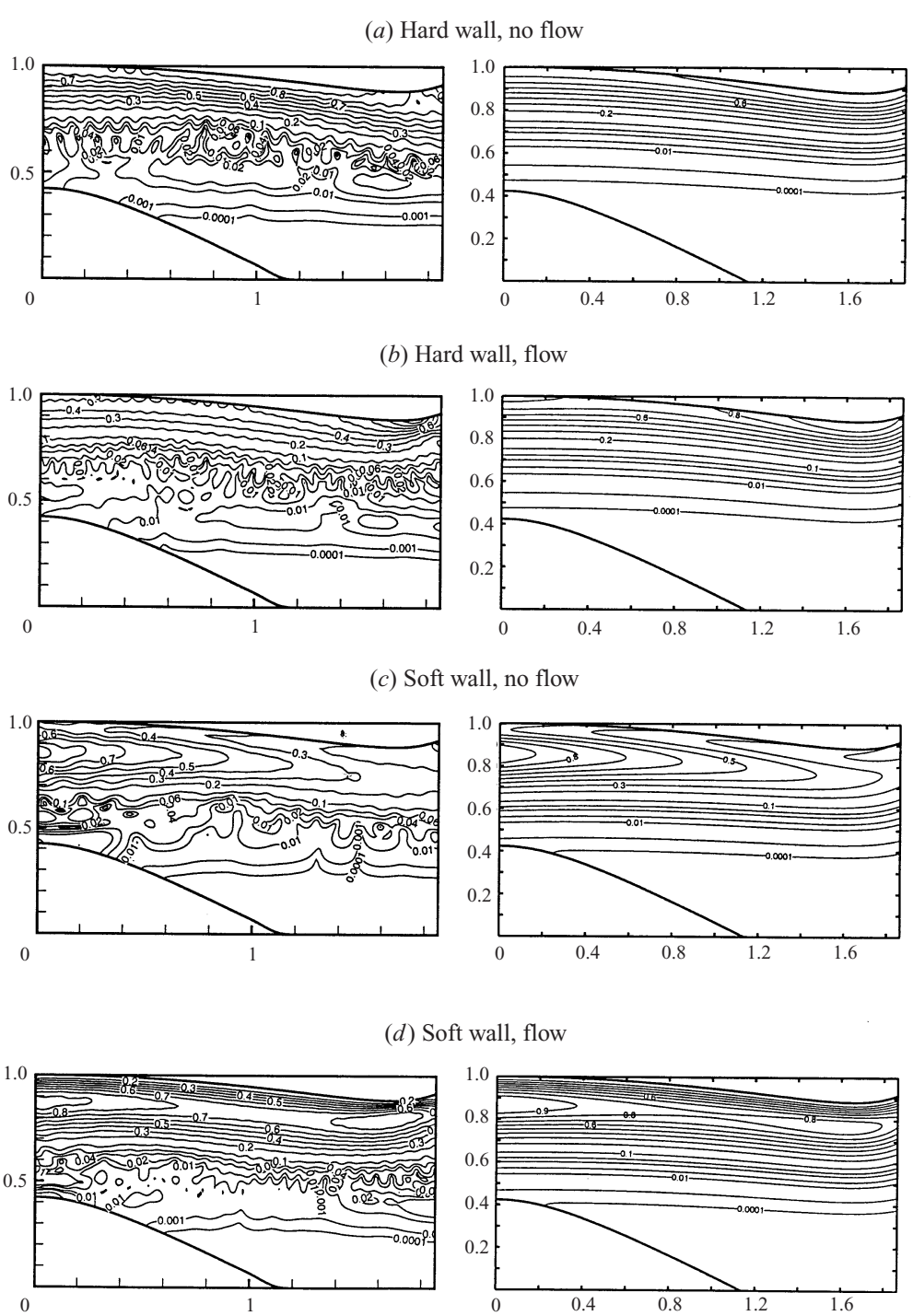

FIGURE 8. As figure 5 but for $m = 20$ and $\omega = 50$.

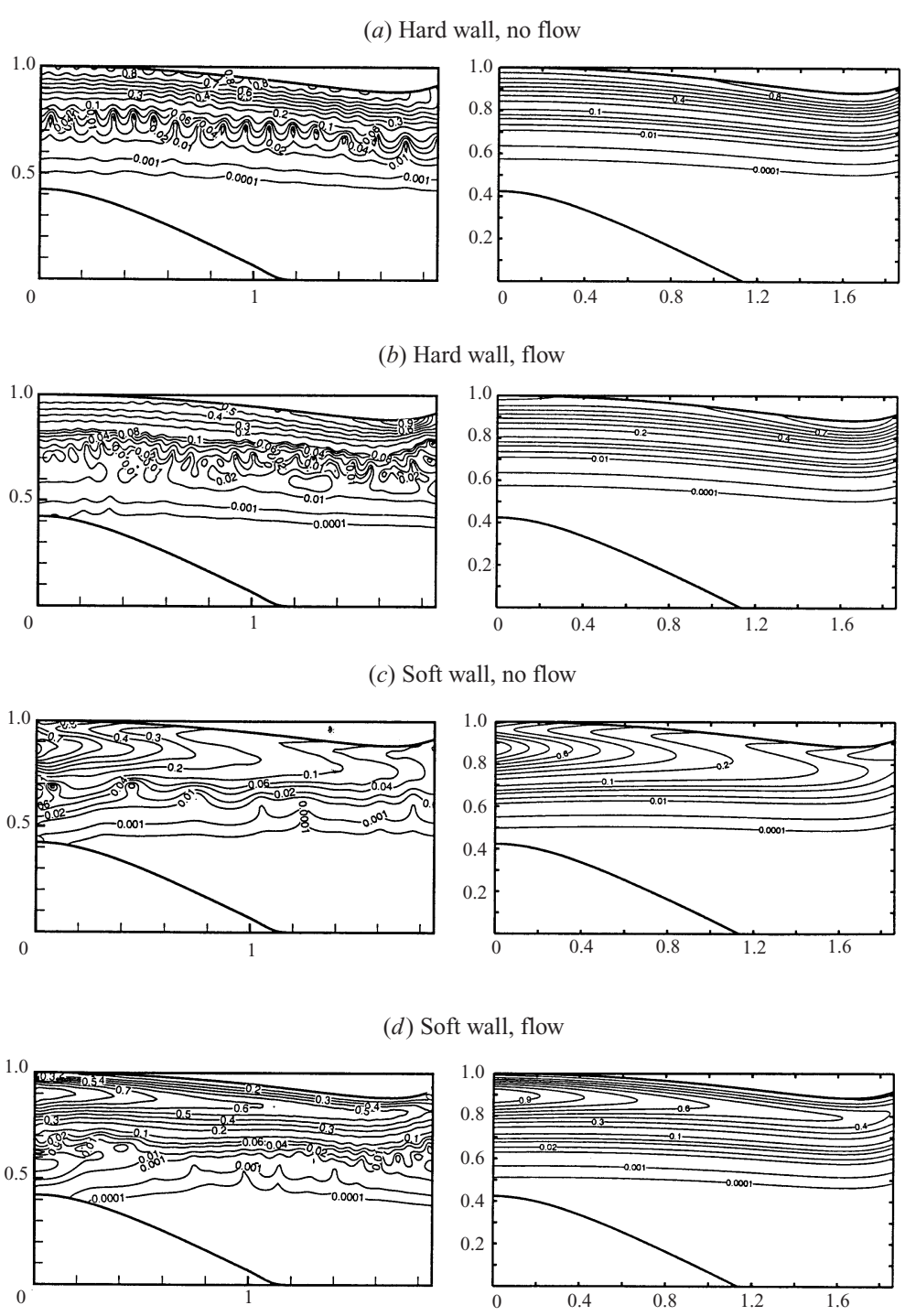

FIGURE 9. As figure 5 but for $m = 30$ and $\omega = 50$.

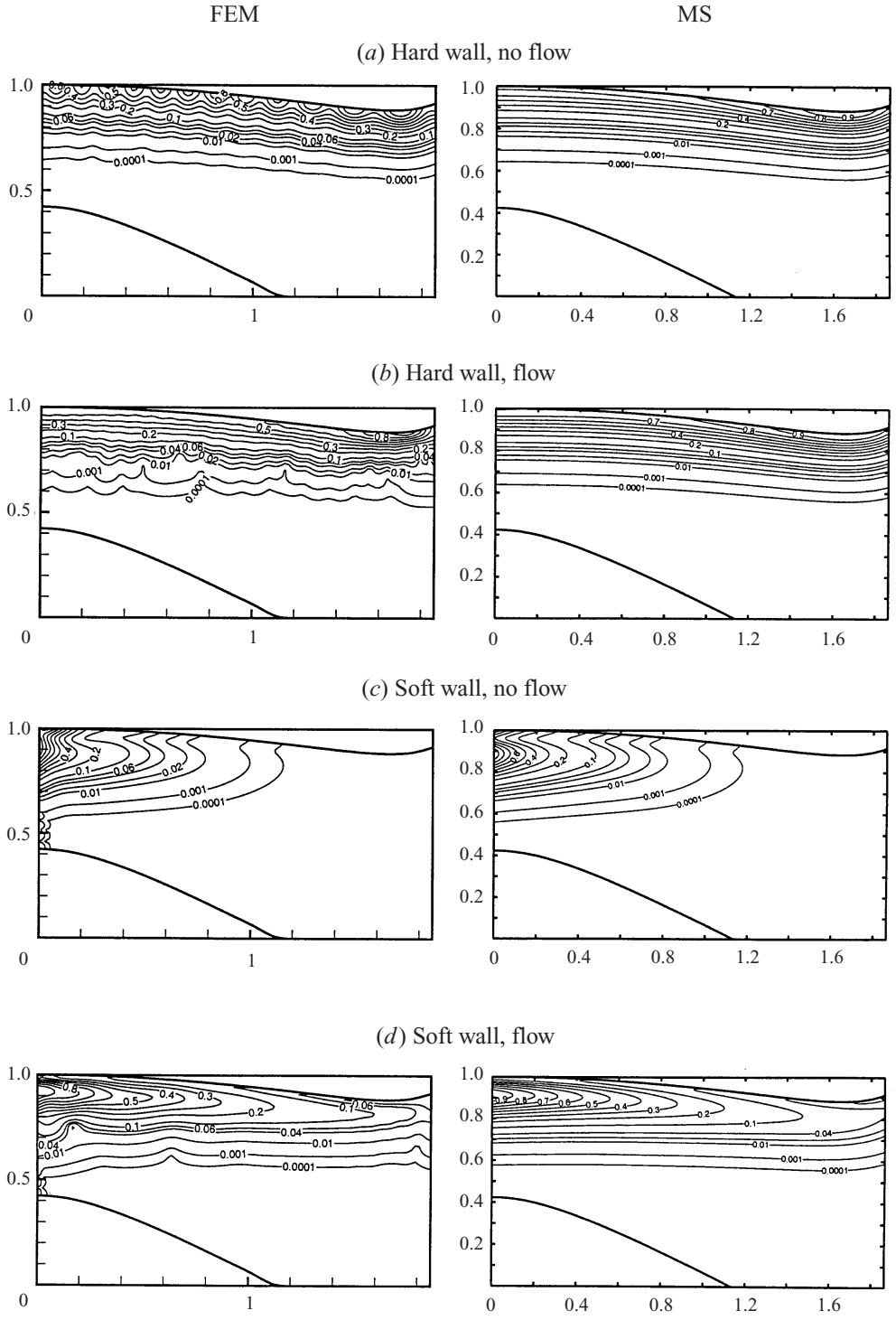

FIGURE 10. As figure 5 but for $m = 40$ and $\omega = 50$.

Figure	m	ω	Ma	FEM	MS	HW cut-on	Cut-off ratio
5(c)	10	10	0	—	120 dB	0	0.87
5(d)	10	10	−0.5	—	164 dB	0	0.85
6(c)	10	16	0	51.6 dB	51.6 dB	1	1.36
6(d)	10	16	−0.5	27.2 dB	27.1 dB	2	1.25
7(c)	10	50	0	4.7 dB	3.5 dB	9	3.38
7(d)	10	50	−0.5	1.5 dB	0.9 dB	11	3.97
8(c)	20	50	0	12.5 dB	12.3 dB	8	1.91
8(d)	20	50	−0.5	3.9 dB	3.3 dB	9	2.26
9(c)	30	50	0	29.0 dB	28.7 dB	4	1.34
9(d)	30	50	−0.5	9.7 dB	8.9 dB	6	1.59
10(c)	40	50	0	196 dB	210 dB	2	1.03
10(d)	40	50	−0.5	28.4 dB	28.6 dB	3	1.23

TABLE 1. Summary of observed net attenuation in soft-wall cases, including the number of hard-wall (HW) cut-on modes and the cut-off ratio of the incident soft-wall mode at $x = 0$.

described by Bessel functions) requires some care. We plan, however, to do it in the near future.

For the soft walls the predicted attenuation (10 log of ratio of acoustic power through source and inlet plane) is given in table 1. For the hard walls the attenuation is either zero (mode is cut on) or infinite (mode is cut off and reflection is negligible). In addition table 1 gives the number of hard-wall cut-on modes at the source plane, the cut-off ratio of the respective incident soft-wall mode. Cut-off ratio is a measure of the angle of the normal to the wave front of the mode relative to the duct axis (Tyler & Sofrin 1962; Rice 1979), and is defined in our notation as

$$\xi = \frac{\omega}{\sqrt{(C_0^2 - U_0^2)\mathrm{Re}(\alpha^2)}}.$$

It extends the meaning of cut-on (propagating) and cut-off (evanescent) for hard-wall modes to soft-wall modes. A mode is cut on if the cut-off ratio is larger than unity and cut off if the cut-off ratio is less than unity.

Although not conclusive in all cases, the general trend seems to be that a high dimensionless frequency ω and a large number of hard-wall cut-on modes, together with a high cut-off ratio ξ, produces the largest difference in attenuation. As will be shown by the iso-pressure contour plots, this is probably due to forward modal scattering.

The possible differences between FEM and MS are due to the following errors or modelling discrepancies.

1. The approximation error of $O(\varepsilon^2)$. For this we need an estimate of ε. Suitable is a typical value of $(\mathrm{d}/\mathrm{d}x)R_2 = \varepsilon(\mathrm{d}/\mathrm{d}X)R_2 = O(\varepsilon)$. From formula (6) it appears that R_2' varies between −0.12 and 0.12 along [0,1.75], but increases to 0.4 in the lip region $[1.75, L]$. If we take $\varepsilon = 0.1$, the estimated approximation error is a few percent.

2. The relatively large wavenumbers in the high-frequency cases with $\omega = 50$. Here we do not have two, but in fact three different length scales: the acoustic wavelengths, the duct radius, and the typical axial length of duct variations. At first sight, a short acoustic length scale would not necessarily have to interfere with the assumption of slow duct variations. However, terms like $\varepsilon\omega$ and $\varepsilon\mu$ do occur in terms of higher order, and there appears to be an effect of forward modal scattering (violating the

WKB assumption) if several well cut-on modes are available, and the primary mode is easily scattered into others.

3. Small but inherent reflection in the FEM at the inlet plane and lip region. It is difficult to assess this contribution because it occurs only together with the intermodal scattering among forward propagating modes (error type 2), since a highly attenuated mode does not produce a significant reflection. Probably, some is visible in figures 6(*a*) and 6(*b*). The average trend, however, does not seem affected.

4. Not exactly the same source in soft-wall cases. FEM uses a source defined by an expansion in a finite number (15) of hard-wall modes, being a small distance ($\frac{1}{100}L$) away from the lined section. Residues of possible mismatch may be visible in figures 6(*d*), 9(*c*, *d*), 10(*c*, *d*). We have experimented with several versions, but the effect on the attenuation was small.

5. Slightly different mean flow. In MS the mean flow field is approximated to the same level as the acoustic field. However, as is seen in figure 4, in the FEM solution also the mean flow is nearly parallel, and the estimated error of $\varepsilon^2 \sim 1\%$ seems to apply here.

For the cases of figure 5(*a–d*) ($m = 10$, $\omega = 10$) the agreement of iso-pressure contours is excellent. None of the above errors play a role. These cases share the characteristic of very high attenuation. Hard-wall modes are deeply cut off. While there is no exact cut-off for soft-wall modes, they have very large attenuation. In the hard-wall cases of figure 5(*a*, *b*) no attenuation is given for either the MS or FEM results. In the MS case, the acoustic power is zero. In the FEM case acoustic power is extremely small (non-zero due only to cut-off mode interaction), but attenuation cannot be reliably calculated because the large decay in acoustic pressure amplitude (note the scaling on the iso-pressure contours) is beyond the resolution achievable. In soft-wall cases of figure 5(*c*, *d*), no attenuation is reported for the FEM results, since as noted above, it is beyond the resolution achievable.

For the series ($m = 10$, $\omega = 16$) of figure 6, with 1 or 2 modes cut on, the agreement is good in the iso-contour plots, and almost perfect in attenuation. Some wiggles are visible in figure 6(*b*), probably due to error type 3.

The high-frequency series ($m = 10$, $\omega = 50$) of figure 7 has very low acoustic pressure values near the duct axis, and many radial modes cut on (9 and 11 at the source plane). We see strong interference with these higher modes. The important region near the outer wall, however, is in very good agreement, but the attenuation differs by an amount of about 1 dB due to error type 2.

For higher m (20, 30, 40) the agreement improves again, although in the iso-contour plots of the FEM results wiggles remain visible due to interference with other modes. The comparable attenuations of figure 10(*c*) (195 dB and 210 dB) are perhaps fortunate, since once again the FEM result is beyond achievable resolution. Even though the incident mode is cut on, there is rapid decay in acoustic pressure (note the scaling of the iso-pressure contours).

8. Conclusions

Any selection of test cases is necessarily limited. It would have been easy to create a more or a less favourable comparison, by making a suitable selection of geometry and parameters. This is not done here. We have defined the test runs entirely on the basis of their relevance to turbofan engine inlet duct applications, and we have not skipped unfavourable cases afterwards. The only restriction we made was that no cut-on/off transition in the hard-walled duct be present. This phenomenon is not yet

implemented in the analytical solution, while at the same time, of course, it is absent in any lined duct.

So considering the fact that the cases are likely to be a representative cross-section of reality, we think the conclusion is justified that the MS and FEM solutions compare favourably, both in iso-pressure contours and in predicted attenuation. Principal differences are related to intermodal scattering at high frequencies, scattering at the inlet plane, and input mode synthesis. The best results are obtained with lining (reducing the importance of reflection) and when the modal structure permits few or no cut-on scattered modes. The attenuation differs in general between a few tenths of a dB and 1 dB.

The correlation shows that MS is definitely useful in applications for assessing liner performance in realistic geometries. Both extending the theory, and further comparison with FEM, for example with an MS implementation that includes a complete modal spectrum and open end reflection, is therefore to be recommended.

The contribution of Professor Eversman was partially supported by NASA Lewis Research Center under Grant NAG 3-2109.

REFERENCES

Astley, R. J. & Eversman, W. 1983 Finite element formulations for acoustical radiation. *J. Sound Vib.* **88**, 47–64.

Danda Roy, I. & Eversman, W. 1995 Improved finite element modeling of the turbofan engine inlet radiation problem. *ASME J. Vib. Acoust.* **117**, 109–115.

Eversman, W. 1991 Aeroacoustics of Flight Vehicles: Theory and Practice. *Volume 2:* Noise Control. Theoretical models for duct acoustic propagation and radiation. *NASA Reference Publication 1258.*

Eversman, W. 2001*a* A reverse flow theorem and acoustic reciprocity in compressible potential flows. *J. Sound Vib.* accepted for publication.

Eversman, W. 2001*b* The boundary condition at an impedance wall in a nonuniform duct with potential flow. *J. Sound Vib.* accepted for publication.

Eversman, W. & Baumeister, K. J. 1986 Modeling wind tunnel wall effects on the radiation characteristics of acoustic sources. *J. Aircraft* **23**, 455–463.

Eversman, W. & Okunbor, D. 1998 Aft fan duct acoustic radiation. *J. Sound Vib.* **213**, 235–257.

Eversman, W., Parrett, A. V., Preisser, J. S. & Silcox, R. J. 1985 Contributions to the finite element solution of the fan noise radiation problem. *ASME J. Vib., Acoustics, Stress, Reliability in Design* **107**, 216–223.

Myers, M. K. 1980 On the acoustic boundary condition in the presence of flow. *J. Sound Vib.* **71**, 429–434.

Parrett, A. V. & Eversman, W. 1986 Wave envelope and finite element approximations for turbo-fan noise radiation in flight. *AIAA J.* **24**, 753–759.

Rice, E. J. 1979 Optimum wall impedance for spinning modes – a correlation with mode cutoff ratio. *J. Aircraft* **16**, 336–343.

Rienstra, S. W. 1998 Sound transmission in slowly varying circular and annular ducts with flow. *AIAA Paper* 98-2311.

Rienstra, S. W. 1999 Sound transmission in slowly varying circular and annular ducts with flow. *J. Fluid Mech.* **380**, 279–296.

Tyler, J. M. & Sofrin, T. G. 1962 Axial flow compressor studies. *Trans. Soc. Automotive Engrs* **70**, 309–332.